



**HAL**  
open science

# A New Multi-Method Assessment of Stratospheric Sulfur Load From the Okmok II Caldera-Forming Eruption of 43 BCE

Ally Peccia, Yves Moussallam, Terry Plank, Kevin Dallasanta, Lorenzo Polvani, Alain Burgisser, Jessica Larsen, Janet Schaefer

► **To cite this version:**

Ally Peccia, Yves Moussallam, Terry Plank, Kevin Dallasanta, Lorenzo Polvani, et al.. A New Multi-Method Assessment of Stratospheric Sulfur Load From the Okmok II Caldera-Forming Eruption of 43 BCE. *Geophysical Research Letters*, 2023, 50 (21), pp.e2023GL103334. 10.1029/2023GL103334 . hal-04273569

**HAL Id: hal-04273569**

**<https://hal.science/hal-04273569v1>**

Submitted on 7 Nov 2023

**HAL** is a multi-disciplinary open access archive for the deposit and dissemination of scientific research documents, whether they are published or not. The documents may come from teaching and research institutions in France or abroad, or from public or private research centers.

L'archive ouverte pluridisciplinaire **HAL**, est destinée au dépôt et à la diffusion de documents scientifiques de niveau recherche, publiés ou non, émanant des établissements d'enseignement et de recherche français ou étrangers, des laboratoires publics ou privés.



Distributed under a Creative Commons Attribution - NoDerivatives 4.0 International License

# **A New Multi-Method Assessment of Stratospheric Sulfur Load from the Okmok II Caldera-Forming Eruption of 43 BCE**

**Ally Peccia<sup>1,2</sup>, Yves Moussallam<sup>1,2</sup>, Terry Plank<sup>1,2</sup>, Kevin DallaSanta<sup>3,4</sup>, Lorenzo Polvani<sup>1,2,3</sup>, Alain Burgisser<sup>5</sup>, Jessica Larsen<sup>6</sup> and Janet Schaefer<sup>7</sup>**

<sup>1</sup>Lamont-Doherty Earth Observatory, Columbia University, Palisades, NY 10964

<sup>2</sup>Department of Earth and Environmental Sciences, Columbia University, Palisades, NY 10964

<sup>3</sup>Department of Applied Physics and Applied Mathematics, Columbia University, New York, NY, USA

<sup>4</sup>NASA Goddard Institute for Space Studies, New York, New York, USA

<sup>5</sup>Univ. Grenoble Alpes, Univ. Savoie Mont Blanc, CNRS, IRD, IFSTTAR, ISTerre, 38000 Grenoble, France

<sup>6</sup>Geophysical Institute, Department of Geosciences, Alaska Volcano Observatory, University of Alaska, Fairbanks, Fairbanks, AK, 99775, USA

<sup>7</sup>Alaska Volcano Observatory, State of Alaska Division of Geological and Geophysical Surveys, Fairbanks, AK, 99709, USA

Corresponding author: Ally S. Peccia ([asp2201@columbia.edu](mailto:asp2201@columbia.edu))

## **Key Points:**

- Petrologic evidence suggests a total of 62 Tg S was released in the caldera-forming eruption of Okmok Volcano in 43 BCE
- Climate models respond linearly to stratospheric sulfur loads. 1-2°C cooling from proxy records suggests 16-32 Tg S injection
- A physical model constrains the proportion of stratospheric sulfur to 2.5-25%; thus we find a common range for all methods of 15-16 Tg S

## 24 **Abstract**

25 The 43 BCE eruption of Okmok Volcano has been proposed to have had a significant climate  
26 cooling impact in the Northern Hemisphere. In this study, we quantify the climate cooling  
27 potential of the Okmok II eruption by measuring sulfur concentration in melt inclusions (up to  
28 1606 ppm) and matrix glasses and estimate a total of  $62 \pm 16$  Tg S released. The proportion  
29 reaching the stratosphere (2.5-25%, i.e., 1.5 – 15.5 Tg S) was constrained by physical modeling  
30 of the caldera-collapse eruption. Using the NASA GISS E2.2 climate model we found a linear  
31 response between cooling and stratospheric sulfur load (0.05-0.08°C/Tg S). Thus, the 1-2°C of  
32 cooling derived from proxy records would require 16-32 Tg sulfur injection. This study  
33 underscores the importance of combining approaches to estimate stratospheric S load. For  
34 Okmok II, we find all methods are consistent with a range of 15-16 Tg S.

## 35 **Plain Language Summary**

36 Gaseous sulfur released in explosive volcanic eruptions can reflect incoming solar radiation in  
37 the stratosphere and cool the Earth's surface. Here, we calculate the total amount of sulfur  
38 released in the 43 BCE caldera-forming eruption of Okmok Volcano, Alaska by measuring the  
39 concentration of sulfur dissolved in magma prior to the eruption. We find that the total sulfur  
40 load from the Okmok II eruption is one of the largest in the last 2500 years, and we use climate  
41 models to simulate cooling and precipitation anomalies associated with total or partial injection  
42 of volcanic sulfur into the stratosphere. However, the estimated sulfur load is larger than that  
43 predicted by sulfur signals preserved in ice cores, and physical modeling of the eruption suggests  
44 that only a proportion of the sulfur released reached stratospheric altitudes. Further, comparison  
45 of temperature reconstructions from tree ring and cave deposit proxies with climate model results  
46 show the cooling associated with the eruption requires only a fraction of the total sulfur load.  
47 Thus, we propose that only a quarter of the total sulfur released in the eruption made it to the  
48 stratosphere, responsible for 1-2°C of cooling in the year following the eruption.

## 49 **1 Introduction**

50 What will be the climate impact of the next major volcanic eruption? The answer to this question  
51 lies in our understanding of past notable events. Here we explore the volcanic drivers and  
52 climatic response of the Okmok II eruption, Alaska. This eruption was recently recognized by  
53 McConnell et al. (2020) as the source of Greenland ice core sulfate peaks at 43 BCE, and  
54 implicated as the cause for regional temperature and precipitation anomalies that may have led to  
55 social unrest in the late Roman Republic and Ptolemaic Kingdom.

56 Okmok II consisted of two eruptive phases, the first producing  $\sim 0.85$  km<sup>3</sup> bulk (0.6 km<sup>3</sup> DRE) of  
57 Plinian rhyodacite and subsequent andesite fall deposits across Umnak Island, and the second  
58 major caldera-forming phase producing  $\sim 50$  km<sup>3</sup> bulk (29 km<sup>3</sup> DRE) of pyroclastic density  
59 current (PDC) deposits (Larsen et al., 2007; Burgisser 2005; Wolfe 2001). The composition of  
60 the tephra recovered from the GISP2 ice core aligns best with the material erupted as basaltic  
61 andesite PDCs (McConnell et al., 2020 and see below). This suggests that the PDC material was  
62 lofted high enough to be dispersed to the opposite side of the Northern Hemisphere, prompting  
63 further study of pyroclastic-associated plumes and caldera collapse via physical modeling  
64 (Burgisser et al., submitted).

65 The primary goal of this study is to provide the first petrological measurements of the total  
66 amount of sulfur released by Okmok II magma. The other goal is to estimate the fraction of this

67 load injected to the stratosphere, critical to determining its climate impact. This quantity is  
68 challenging to determine by any one method, and the novelty of our study is that we employ  
69 three independent methods and datasets for estimating stratospheric sulfur: 1) ice sheet  
70 deposition and sulfur isotopes, 2) global climate model and climate proxy data, and 3) total  
71 petrologic sulfur load and eruption dynamics modeling for stratospheric injection.

## 72 **2 Materials and Methods**

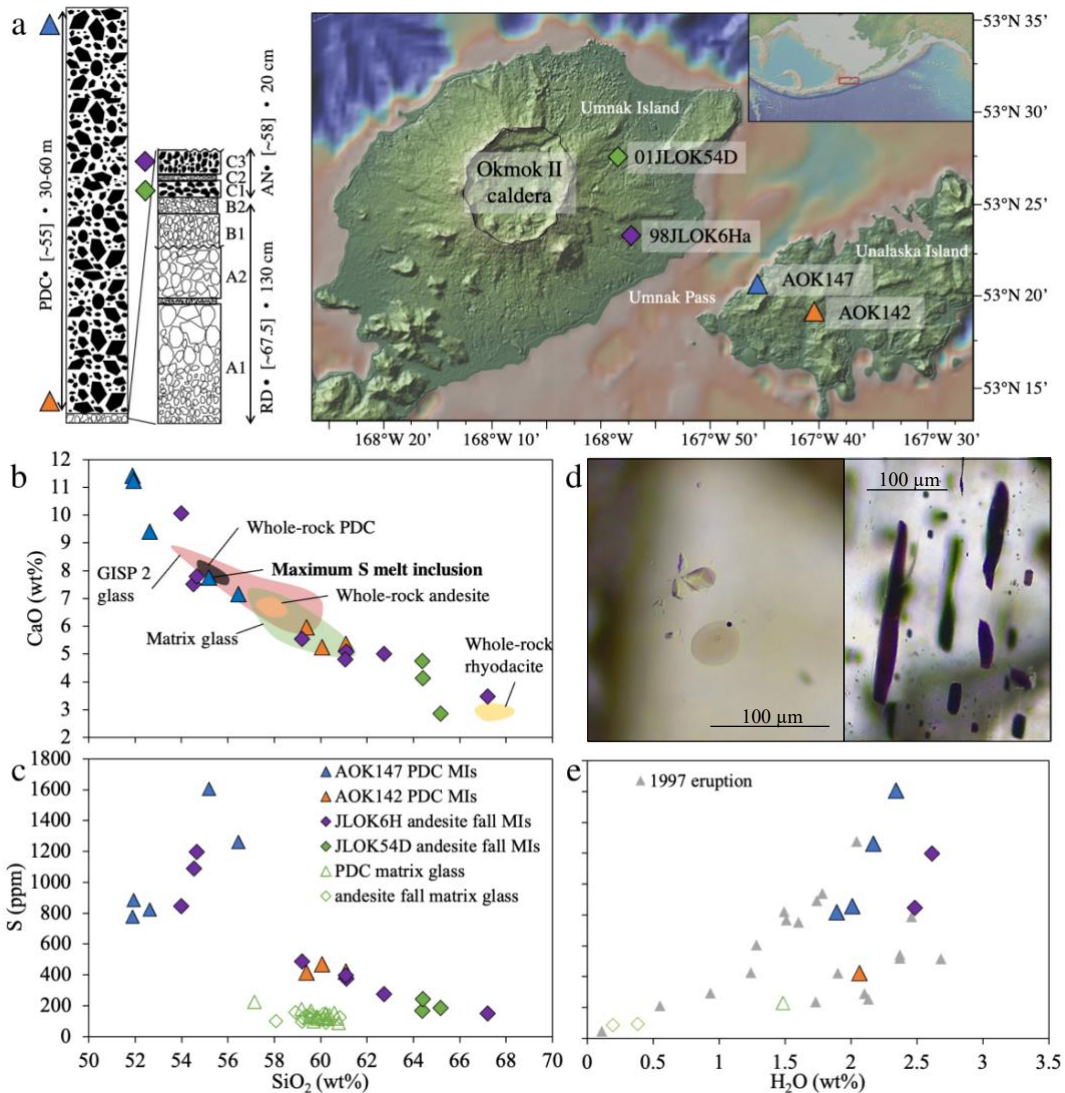
73 Okmok II PDC and andesite fall were selected for melt inclusion study (Fig. 1a; Table S3).  
74 Polished crystals and matrix glasses from four samples were measured by electron microprobe  
75 for major element composition and sulfur concentration. Selected melt inclusions and matrix  
76 glasses were then measured for water and sulfur content by ion microprobe (Fig. 1d; Text S3-  
77 S4).

78 To quantify the climate impacts of different stratospheric sulfur injection amplitudes, we  
79 simulated the effect of the Okmok II eruption on the global climate system using the NASA  
80 Goddard Institute for Space Studies (GISS) Model E2.2 (Rind et al., 2020, Orbe et al., 2020). It  
81 was configured following DallaSanta & Polvani (2022) and is a state of the art atmosphere-  
82 ocean-land-sea ice coupled model which participated in the Coupled Model Intercomparison  
83 Project, Phase 6 (CMIP6) (Text S7).

## 84 **3 Total sulfur load**

### 85 **3.1 Melt inclusion composition**

86 The sulfur concentrations in 19 melt inclusions from Okmok II range from 152 to 1606 ppm S  
87 (with 10% relative uncertainty in the ionprobe analysis) in melt compositions that span from  
88 basaltic to rhyodacitic (51–65 wt% SiO<sub>2</sub>, concentrations expressed volatile-free). To estimate  
89 sulfur load, it is critical to determine the melt inclusion compositions that best reflects the ~ 50  
90 km<sup>3</sup> of bulk PDC magma, as both the whole rocks and matrix glasses are degassed in sulfur. The  
91 more evolved composition of the GISP2 tephra (54.7-59.9 wt% SiO<sub>2</sub>) and PDC matrix glass  
92 (57.1-60.8 wt% SiO<sub>2</sub>) is inferred to be the result of degassing-driven crystallization of microlites  
93 upon ascent as described by Larsen et al. (2007), and thus does not represent the bulk PDC  
94 composition (Fig. 1b; Text S5). The MI compositions in AOK147-plag have SiO<sub>2</sub> (55.2-56.4  
95 wt%) that overlap best with the PDC whole rocks (54.6-55.7 wt% SiO<sub>2</sub>), which we take to best  
96 represent the bulk composition of the PDC magma (Fig. 1b). These inclusions have the highest  
97 sulfur concentrations and are in equilibrium with their plagioclase hosts and the bulk PDC  
98 composition, suggesting they represent the original volatile content of the magma before  
99 degassing, with sulfide saturation inferred from the Cu-Th trend in Okmok whole rocks (1263-  
100 1606 ppm S, Fig. 1c, Text S6). Selection of these inculsions is critical in accounting for the  
101 sulfur concentration in the parental PDC magma body at depth, which would otherwise be  
102 underestimated by ~1000 ppm S if the petrologic method was applied to melt inclusions similar  
103 in composition to the matrix glass (Su et al., 2016; Fig. 1c). We thus take the pre-eruptive  
104 concentration for the Okmok II PDC magma as the maximum sulfur measured in these  
105 inclusions: 1606 ± 160 ppm. Total sulfur concentration in the parental PDC magma could be  
106 even higher due to minor sulfide fractionation (see Cu-Th systematics in Fig. S4) or prior  
107 degassing.



108

109 **Figure 1.** Stratigraphic sequence of Okmok II units (a, left) and map of sample locations across  
 110 Umnak and Unalaska Islands (a, right). Units are labeled by type and composition (RD =  
 111 rhyodacite fall, AN = andesite fall, PDC = pyroclastic density current), with bulk rock SiO<sub>2</sub> wt%  
 112 in brackets. Fall deposits are noted by units (A, B, C) identified in Burgisser et al. (2005), and  
 113 are scaled relative to maximum deposit thickness. Pyroclastic flow facies have an average  
 114 thickness of 30-60 m depending on distance from the caldera. Panels b and c show sulfur and  
 115 major element concentrations in melt inclusions, matrix glasses, and whole-rocks from Okmok  
 116 II. CaO and SiO<sub>2</sub> are reported volatile-free, normalized to 100%. Matrix glasses are plotted  
 117 together in (b), and separated in (c). They largely overlap in our data set. Photomicrographs (d)  
 118 are of representative olivine-hosted melt inclusions from the JLOK6H andesite fall (left) and  
 119 plagioclase-hosted melt inclusions from PDC deposit sample AOK147 (which contains the  
 120 maximum S concentrations). The H<sub>2</sub>O and S concentrations in (e) were measured by ionprobe,  
 121 and include melt inclusion measurements from the 1997 eruption of Okmok from Zimmer et al.,  
 122 (2010). Panel (a) made with GeoMapApp (Ryan et al., 2009).

### 123 3.2 Total mass erupted and total sulfur load

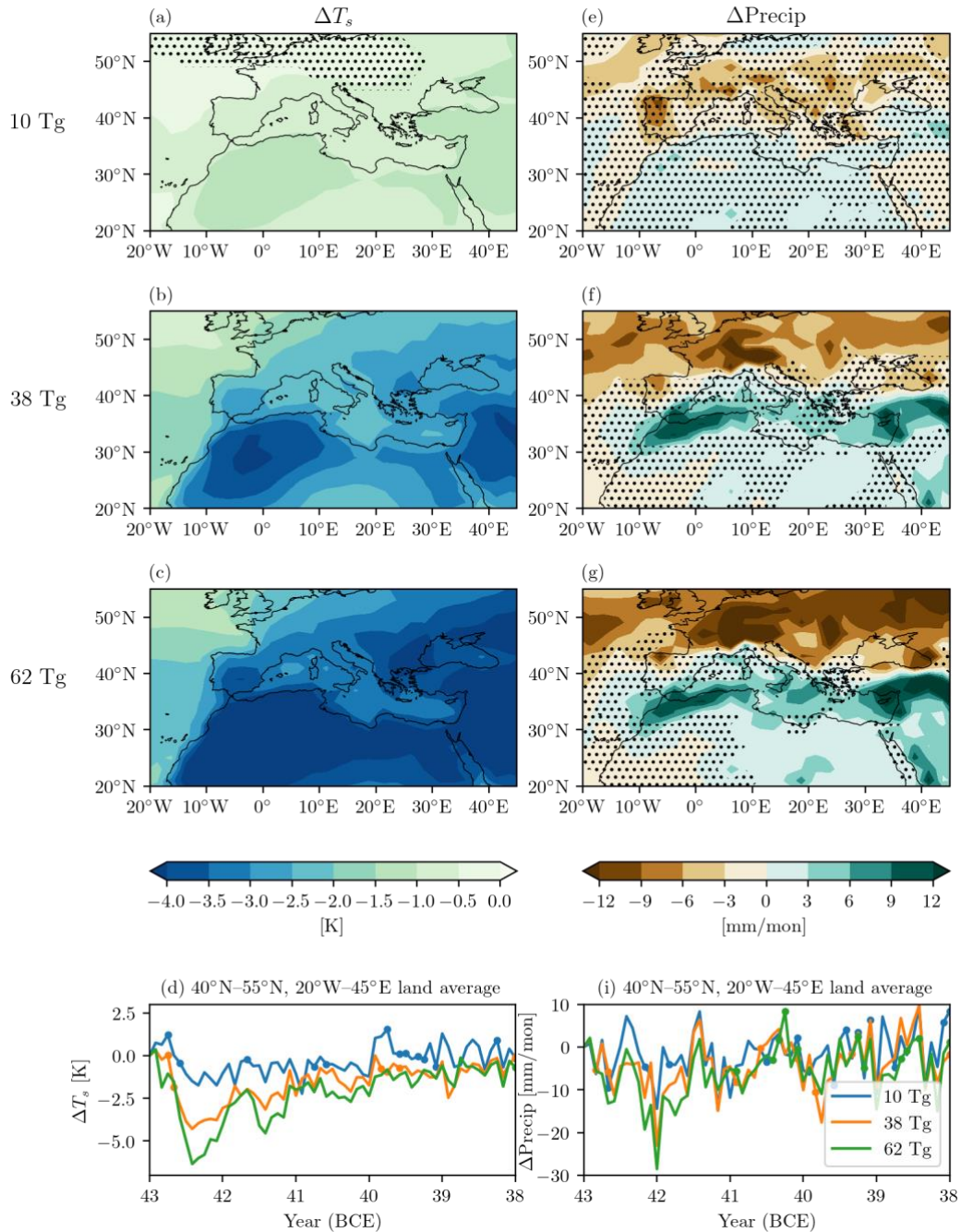
124 Calculating the total sulfur load from Okmok II requires an estimate of the erupted mass. PDCs  
 125 account for 98% of the volume erupted in Okmok II, and thus represent the most important  
 126 volume component for estimating total sulfur load. Burgisser (2005) estimated a total of 24 km<sup>3</sup>  
 127 of PDC deposits on Umnak and Unalaska Island, but recognized a large uncertainty in the  
 128 volume of underwater deposits. To address this, we assume two areas of deposition around  
 129 Umnak Island that extend the thickness of the deposits measured on land to sea (see Fig. S3).  
 130 This produces an additional 25 km<sup>3</sup> of pyroclastic flows deposited underwater for a total volume  
 131 during Okmok II PDC stage of 50 ± 10 km<sup>3</sup>, consistent with the volume of the caldera (Burgisser  
 132 2005). We calculate a total erupted magma mass of 4.29 ± 1.01 × 10<sup>13</sup> kg, based on average  
 133 deposit density and corrections for pre-existing lithic material and deposit void fraction  
 134 (Burgisser, 2005; Text S1). The sulfur load is then derived from Eqn (1) of Devine et al. (1984):

$$135 \quad M_s = M_v(1 - W_x)(C_i - C_m) \quad (1)$$

136 where  $M_s$  is the mass of sulfur erupted,  $W_x$  is the mass fraction of crystals,  $C_i$  is the concentration  
 137 of sulfur as measured in melt inclusions, and  $C_m$  is the concentration of sulfur as measured in  
 138 degassed matrix glass.  $W_x$  is taken as 1.7 ± 1.8% (Burgisser, 2005).  $C_i$  is 1606 ± 160 ppm (as  
 139 above) and  $C_m$  is 127 ± 23 ppm S. Thus, ~1500 ppm of sulfur was degassed during this eruption,  
 140 producing a total sulfur load of 62 ± 16 Tg S (Eq. 1, Table S1). This is likely a minimum  
 141 estimate for total Okmok II sulfur emission, given our assumptions of zero pre-*ex*solved gas  
 142 phase. Further, seawater vaporization as a result of contact with hot PDC material could have led  
 143 to additional S release (Rowell et al., 2022), though it's unlikely that this source would reach a  
 144 significant altitude (Dufek et al, 2007).

### 145 3.3 Climate model scenarios

146 We performed model simulations to study the effect of three different stratospheric S loads: 62  
 147 Tg (total petrologic S load), 38 Tg (estimated by McConnell et al., 2020 from ice core load), and  
 148 10 Tg (lower bound) and averaged response over 43 and 42 BCE, when the signal is largest (Fig.  
 149 2d). In the Mediterranean region, the magnitude of cooling ranges from 1K to 4K (Fig. 2a-c).  
 150 Land surface cooling observed with 38 Tg S agree closely with McConnell et al. (2020), who  
 151 used a different climate model than ours, but an identical aerosol forcing model. Over the  
 152 Northern Hemisphere (Fig. S1a-d), we observe highly significant surface temperature responses.  
 153 The milder responses over Northern Eurasia, as compared to North America, are associated with  
 154 a positive phase of the Northern Annular Mode in boreal winter, which emerges for sufficiently  
 155 large eruptions (DallaSanta & Polvani 2022). The lack of response in the Southern Hemisphere  
 156 is due to the Easy Volcanic Aerosol (EVA) parameterization of hemispheric asymmetry, though  
 157 a small volcanic sulfate peak is observed in Antarctic ice cores around the same time (Fig. S1;  
 158 Toohey et al., 2016). Notably, the climate response, as defined by the ensemble averaged  
 159 departure from control run, shows roughly linear cooling as a function of S load (0.05-0.08°C  
 160 cooling/Tg S) (Fig. 4).



161

162 **Figure 2.** Impact of Okmok II eruption on Mediterranean surface temperature (column 1) and  
 163 precipitation (column 2). The responses are defined as ensemble-averaged departures from the  
 164 corresponding control run, averaged over 43 and 42 BCE. Stippling indicates an inability to  
 165 reject the null hypothesis at 95% confidence. The three sulfate amplitudes are labeled for rows  
 166 1–3. Row 4 shows the time evolution of the responses, averaged over the specified region. Dots  
 167 indicate where all 10 members are less than zero.

168 Overall, we find reduced precipitation over Northern Europe and increased precipitation over  
 169 Southern Europe following the eruption, with magnitudes up to 12 mm/month. Our dipole

170 response for 38 Tg is slightly shifted in latitude from that in McConnell et al. (2020), pointing to  
171 intermodel uncertainties. As with temperature, the precipitation response strengthens  
172 approximately linearly with stratospheric sulfur injection mass, with significance emerging at 38  
173 Tg S (Fig. 2f) and strengthening at 62 Tg S (Fig. 2g). However, the month-to-month spread  
174 across ensemble members is high (Fig. 2h). Thus, the Roman Empire likely experienced overall  
175 precipitation changes after the eruption, but any given month could have been wetter or drier.  
176 The precipitation changes over Africa reflect heightened interannual variability due to  
177 contraction of the Hadley Cell, which could have led to drying at the Nile headwaters (Fig. 2e-i,  
178 Fig. S1e-i), consistent with historical records (McConnell et al., 2020). On a global scale (Fig.  
179 S1e-i), the precipitation response is more robust, associated with changes to the zonally  
180 symmetric circulation.

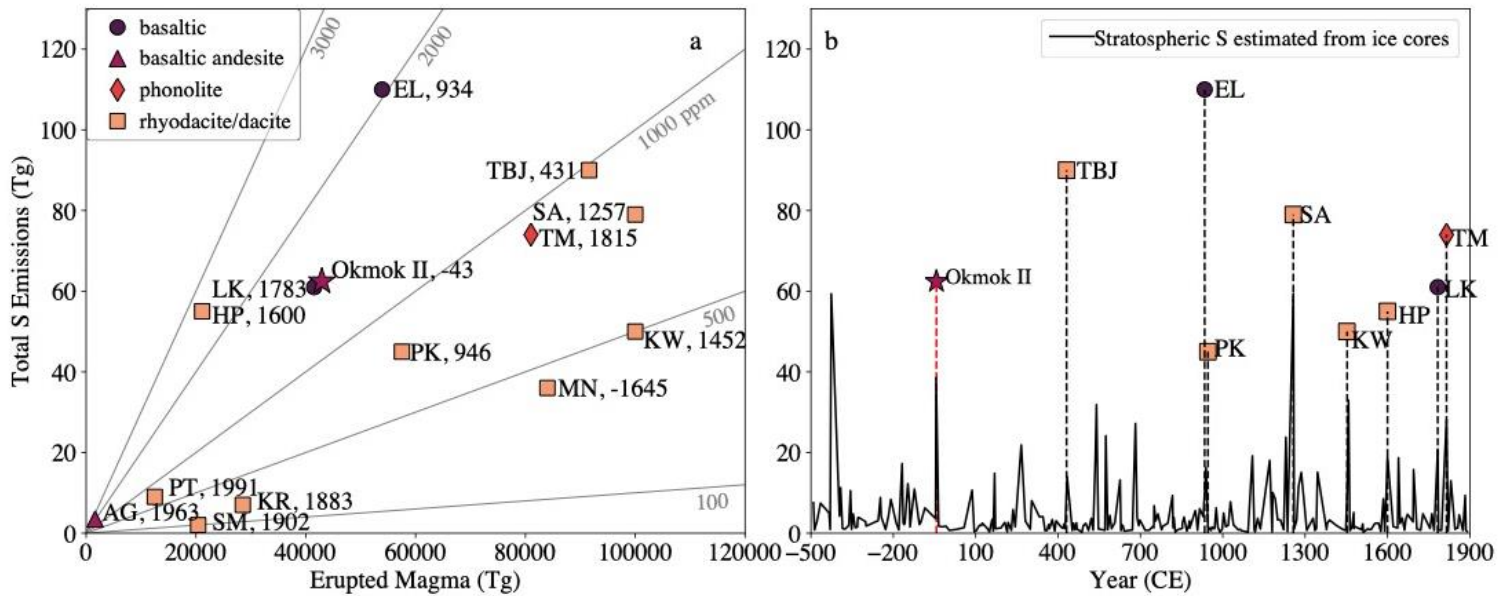
181 Lastly, we find that the month of eruption does not appear to be critical for the temperature and  
182 precipitation impacts (Fig. S2). This provides confidence that our results are meaningful for  
183 historical interpretation, as the actual eruption month of the Okmok II eruption is not known.

#### 184 **4 Multi-method assessment of stratospheric S injection**

##### 185 4.1 Among the largest sulfur loads in history

186 A petrologic sulfur load of 62 Tg S for Okmok II is on par with historical eruptions of similar  
187 size (Laki, Samalas, Paektu, Minoan), and ranks as one the largest volcanic sulfur loads in the  
188 last 2500 years (Fig. 3). Comparable eruptions have been linked to climate instability and major  
189 historical milestones: the 1783 flood-lava eruption of Laki emitted around 60 Tg of sulfur and  
190 drove significant cooling in the Northern Hemisphere (Zambri et al., 2019; Schmidt et al., 2011;  
191 Thordarson and Self, 2003), while the 1257 eruption of Mt. Samalas generated  $\sim 1\text{-}2^\circ\text{C}$  global  
192 cooling and has been connected with the initiation of the Black Death in Europe (Guillet et al.,  
193 2017; Fell et al., 2020; Büntgen et al., 2022). Notably, petrologic evidence suggests very little  
194 halogen degassing from Okmok II ( $\sim 0$  Tg for Cl and F), with matrix glass concentrations of Cl  
195 and F near or greater than that observed in melt inclusions.





196 **Figure 3.** Okmok II sulfur load compared with (a) sulfur emission estimates of other historical  
 197 eruptions (Table S2) and (b) ice core-based estimates of stratospheric sulfur loading (b). Lines in  
 198 (a) show sulfur emissions for magmas that undergo 100, 500, 1000, 2000, and 3000 ppm of  
 199 sulfur degassing, for reference. Dashed lines in panel (b) show the offset between total sulfur  
 200 emission from petrological studies and the stratospheric S estimated from ice core studies. The  
 201 difference between the two likely reflects variable stratospheric injection of the total sulfur load  
 202 during any given eruption. Eruptions are colored by dominant composition, with eruption years  
 203 noted. Dates in (b) extend from 500 BCE to 1990 CE, reflecting the coverage of the ice core  
 204 record presented in the eVol2k v3 database (Toohey and Sigl, 2017). Eruption name codes:  
 205 (AG:Agung, EL:Eldgja, HP:Huayanaputina, LK:Laki, KR:Krakatau, KW:Kuwae,  
 206 MN:Minoan/Thera, PK:Paektu, PT:Pinatubo, SA:Samalas, SM:Santa Maria, TBJ:Ilopango TBJ,  
 207 TM:Tambora).

208 Only S injected into the stratosphere exerts a climate cooling influence (e.g., Robock, 2000).  
 209 Sulfate concentrations in ice cores have been used to estimate stratospheric sulfur loading,  
 210 relying on the transport and deposition of volcanic sulfate aerosols to ice sheets 1-2 years post-  
 211 eruption (Toohey and Sigl, 2017). While this strategy is useful for identifying the timing of large  
 212 eruptions and their relative magnitudes, it does not provide source constraints nor does it  
 213 distinguish stratospheric fall-out vs. tropospherically transported sulfur (Marshall et al., 2021). In  
 214 Figure 3b, we compare petrological estimates of sulfur load and ice core estimates over the past  
 215 2500 years, and find that petrologic estimates are systematically higher than the modeled ice core  
 216 deposition. This offset likely reflects variable stratospheric injection due to the physical

217 dynamics of any given eruption and illustrates the importance of studies of past volcanic sulfur  
218 loads.

219 To address partial stratospheric injection of the total S load from the Okmok II eruption, we  
220 compare below three independent methods: 1) ice core deposition, 2) eruption dynamics, and 3)  
221 climate proxy data.

#### 222 4.2 Stratospheric injection from ice cores

223 Synchronized estimates made by Toohey and Sigl (2017) predict stratospheric sulfur injection of  
224  $38.6 \pm 11.3$  Tg S from Okmok II based on its source location and ice core sulfate concentrations.  
225 McConnell et al. (2020) assumed all of this was stratospheric, and used this as input to their  
226 climate model. A recent study (Pearson et al., 2022) proposes an even larger stratospheric sulfur  
227 load of  $48 \pm 15$  Tg S, which would represent  $\sim 77\%$  of the total erupted sulfur given our  
228 petrologic estimate. This same study, however, makes the important point that some ice-  
229 deposited S will be tropospheric, especially for volcanoes like Okmok which are relatively  
230 proximal to Greenland.

231 A closer examination of mass independent fractionation in sulfur isotopes (S-MIF) may be used  
232 to resolve the stratospheric vs. tropospheric ice deposition of sulfur (Burke et al., 2019). A study  
233 of the Aniakchak II eruption (1628 BCE) uses mass balance, along with triple isotope  
234 measurements of sulfate deposited in Greenland to estimate the proportion of ice-deposited  
235 sulfate that reached the stratosphere (Pearson et al., 2022). The Aniakchak II eruption, which had  
236 a similar ice deposition (52 Tg) to Okmok II (48 Tg) and is at similar latitude in Alaska ( $56.9^\circ\text{N}$ )  
237 to Okmok ( $53.4^\circ\text{N}$ ), deposited a sulfur peak on Greenland that was calculated to be 61%  
238 stratospheric and 39% tropospheric. Given that the magnitude of the S-MIF peak measured for  
239 Okmok was much smaller than that for Aniakchak ( $\Delta^{33}\text{S}_{\text{max}} = 0.20\text{‰}$  for Okmok II vs.  $\Delta^{33}\text{S}_{\text{max}} =$   
240  $1.30\text{‰}$  for Aniakchak II), the stratospheric proportion for the total volcanic S deposited  
241 following the Okmok II eruption will be  $< 61\%$ . As the measurements in McConnell et al. (2020)  
242 did not include key sulfur concentrations or background isotope ratios, it is not currently possible  
243 to carry out a meaningful sulfur mass balance for Okmok. Furthermore, S-MIF may not occur in  
244 the lower stratosphere at high latitudes, and thus relying solely on  $\Delta^{33}\text{S}$  may result in an  
245 underestimation of stratospheric sulfur injection and resulting climate cooling (Thordarson and  
246 Self, 2003). Nonetheless, the existing measurements suggest a smaller stratospheric proportion  
247 for Okmok II vs. Aniakchak II, and thus we can conclude that  $< 29$  Tg (61% of 48 Tg) of Okmok  
248 II sulfur load measured in ice cores was stratospheric. This would constitute  $< 47\%$  of the total S  
249 erupted.

#### 250 4.3 Stratospheric injection from eruption dynamics models

251 The presence of basaltic andesite tephra and S-MIF in Greenland ice cores indicate that the  
252 Okmok II PDC material reached across the Northern Hemisphere and had a stratospheric  
253 component (McConnell et al., 2020). This presents a conundrum, as the Okmok II PDC deposits  
254 are not associated with an airfall deposit. In order to address how a predominantly pyroclastic  
255 flow-generating eruption could also produce stratospheric sulfur and hemispheric ash without

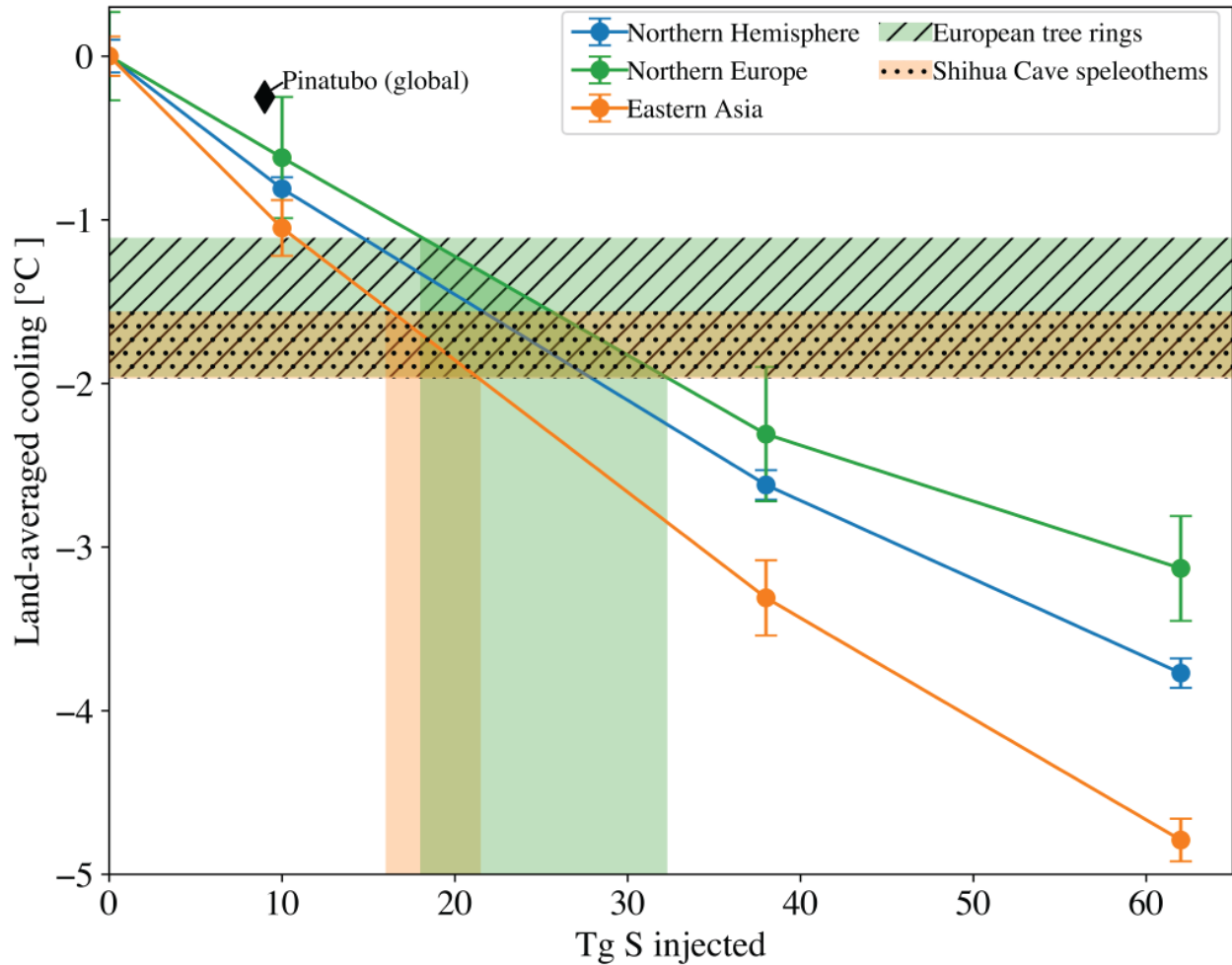
256 producing a Plinian air-fall, a companion study uses a numerical model to explore the conditions  
257 that could lead to this eruptive behavior.

258 Burgisser et al., (submitted) apply the MFIX-TFM two-phase flow model to simulate the  
259 dynamics of PDC emplacement. Model results are constrained by field stratigraphic observations  
260 of asymmetric deposition, maximum flow runout, a lack of airfall deposits and total mass  
261 erupted, with the stratospheric injection of gas during the eruption estimated via mass balance  
262 based on the fraction of stratospheric solids.

263 The results of this physical model indicate that 2.5-25% of the solids and gases from the PDC  
264 phase of the Okmok II eruption would be injected into the stratosphere (Burgisser et al.,  
265 submitted). The low proportion of stratospheric injection reflects the lack of an airfall deposit  
266 from the central plume, with the majority of stratospheric injection occurring via successive  
267 pulses of co-ignimbrite material issued from the main pyroclastic flows. We note that complex  
268 eruption dynamics may also affect the transport of S into the stratosphere, such as scavenging in  
269 a water-rich plume (Thordarson et al., 1996). Nevertheless, if only 2.5 – 25% of the total Okmok  
270 II sulfur is stratospheric, that would result in a stratospheric injection of 1.55 to 15.5 Tg, well  
271 below the 29 Tg maximum outlined above based on ice deposition.

#### 272 4.4 Constraints from climate models and proxies

273 Temperature proxy evidence from tree ring and speleothem records (McConnell et al., 2020; Sigl  
274 et al., 2015) indicate  $> 2^{\circ}\text{C}$  cooling in the Northern Hemisphere around the time of the Okmok II  
275 eruption. As discussed above, our climate modeling indicates a roughly linear relationship  
276 between cooling and mass of S injected into the stratosphere (Fig. 4). Thus, the amount of  
277 cooling recorded by temperature proxies can constrain the amount of stratospheric S needed to  
278 create such a signal.



279

280 **Figure 4.** Land-averaged cooling response following modeled stratospheric sulfur injections (10,  
 281 38, 62 Tg S) from Okmok II over three representative areas: Northern Europe (green line, 40°N-  
 282 70°N, 10°W, 30°E), Asia (orange line, 30°N-55°N, 40°E, 140°E), and the Northern Hemisphere  
 283 (blue line). The three injection scenarios show a roughly linear cooling response for all regions.  
 284 Proxy cooling reconstruction is denoted by the shaded areas: tree ring temperature  
 285 reconstructions from Northern Europe predict  $-1.52 \pm 0.42^\circ\text{C}$  of cooling in 43 BCE (Luterbacher  
 286 et al., 2016), while a Chinese speleothem record predicts  $-1.76 \pm 0.2^\circ\text{C}$  of cooling within a 5-year  
 287 dating uncertainty (Tan et al., 2003). Combined with climate model runs, overlapping proxy  
 288 evidence suggests a stratospheric sulfur load of 18–22 Tg S. Stratospheric sulfur injection and  
 289 observed change in global mean surface temperature from the 1991 eruption of Pinatubo is noted  
 290 for reference (Guo et al., 2004; Pauling et al., 2023).

291 Temperature-sensitive trees in Scandinavia and Austria indicate  $1.52 \pm 0.42$  ( $1\sigma$ )  $^\circ\text{C}$  of cooling in  
 292 43 BCE (Luterbacher et al., 2016). The Shihua Cave temperature reconstruction suggests -  
 293  $1.76 \pm 0.20$  ( $1\sigma$ )  $^\circ\text{C}$  (Tan et al., 2003). Taken together, these proxies indicate a conservative 1.1 to  
 294  $2.0^\circ\text{C}$  of cooling. Comparing the cooling recorded by European trees (1.1 to  $1.9^\circ\text{C}$ ) to the land-  
 295 averaged cooling response over Northern Europe predicted by our model, we infer a  
 296 stratospheric sulfur injection of 18–32 Tg (Fig. 4). The Asia-averaged model applied to the

297 Shihua Cave speleothems suggests 16–22 Tg S injection. The two overlap in the range of  $20 \pm 2$   
298 Tg.

#### 299 4.5 Multi-method convergence of stratospheric S injection

300 The upper limit from the eruption model (15.5 Tg) approaches the lower limit of the climate  
301 model (16 Tg, as discussed above) and both are permissible given the upper bound from ice  
302 deposition (29 Tg). Thus, 15–16 Tg of stratospheric S from Okmok II is consistent with all data,  
303 models and approaches.

304 Despite this coherence, it is worth considering the uncertainties due to the sparsity of data and  
305 number of assumptions. It is possible that additional gaseous sulfur could have been injected  
306 during the rhyodacitic Plinian phase that preceded the PDCs and caldera collapse. However, the  
307 lack of any glass > 60% SiO<sub>2</sub> in the Greenland ice cores is inconsistent with the earlier Plinian  
308 phases producing a major stratospheric load. Alternatively, it is possible that our petrologic  
309 estimate is too low. In order to overlap with the proxy cooling-based estimate for Okmok II (18-  
310 22 Tg S), and assuming a 25% stratospheric portion, the total petrologic load would have to be  
311 increased to 80 Tg S. A higher petrologic load could be achieved with additional MI  
312 measurements that could extend to S concentrations higher than 1600 ppm, although we note that  
313 Zimmer et al. (2010) measured less than 1300 ppm in all 20 MI from several more recent mafic  
314 eruptions of Okmok (Fig. 1e). A less conservative estimate of total eruptive volume, or the  
315 addition of exsolved sulfur from an unerupted primitive parent could also supply an additional  
316 sulfur load.

317 Conversely, the observed climate cooling could be overestimated. Proxy estimates for cooling on  
318 interannual timescales are relatively sparse due to the lack of ancient tree ring records. It is also  
319 questionable how well a regionally-averaged ensemble of climate models might relate to  
320 location-specific (and seasonally-specific) data. The GISS climate model results are also very  
321 likely to depend on the injection height and aerosol size, and the EVA model used here may not  
322 be a good representation of the Okmok II eruption.

323 Regardless, all evidence suggests less than half of the total Okmok II petrologic sulfur load was  
324 injected into the stratosphere, where it produced a significant climate cooling effect. We see the  
325 relative agreement in multiple reconstructions as a success that demonstrates the utility of this  
326 three-pronged approach to evaluate other eruptions with more robust climate proxy data.

## 327 5 Conclusions

328 The Okmok II eruption released a total sulfur load of  $62 \pm 16$  Tg S, one of the largest estimated  
329 sulfur loads in recorded history. However, eruption dynamics models and ice core S-MIF data  
330 suggest that much of the sulfur released during Okmok II did not reach the stratosphere. Thus,  
331 only a fraction of this total load was available to impact surface climate. Comparison of model-  
332 generated climate anomalies with coincident cooling recorded by tree ring and speleothem  
333 proxies suggests that a stratospheric sulfur load of 18-22 Tg is consistent with the observed  
334 climate effect. This constitutes ~30% of the total petrologic sulfur load, in good agreement with

335 the upper end of stratospheric injection predicted by physical modeling (25%) and permissible  
336 given the ice core S-MIF (< 61%).

337 Moreover, we find a systematic mismatch between petrological and ice core estimates of  
338 volcanic sulfur loads, suggesting that partial stratospheric injection should be considered when  
339 examining other large eruptions. Okmok II serves as a case study for an interdisciplinary  
340 approach to reconstructing major historical eruptions and their related impacts – one that  
341 combines petrological source constraints, physical modeling, and climate models to interpret the  
342 ice core record.

### 343 **Acknowledgments**

344 We gratefully acknowledge the Alaska Volcano Observatory and Alaska Geologic Materials  
345 Center repositories for providing samples. We thank Celine Martin, Yunbin Guan, Henry  
346 Towbin, Shuo Ding, and Sarah Shi for assistance in sample preparation and measurement. The  
347 ancestral homelands of the Unangan people include Okmok Volcano. We respect and honor the  
348 past, present, and future Unangan people and their land. The work of Kevin DallaSanta and  
349 Lorenzo Polvani was funded in part by a grant of the U.S. National Science Foundation to  
350 Columbia University. We thank reviewers Bruno Scalliet and Thor Thordarson and editor  
351 Christian Huber for their constructive feedback, which helped to improve this paper.

### 352 **Open Research**

353 The data used for the petrological characterization of Okmok II in this study are available to  
354 download via the EarthChem repository: <https://doi.org/10.26022/IEDA/112955> .

355 **References**

- 356 Büntgen, U., Smith, S. H., Wagner, S., Krusic, P., Esper, J., Piermattei, A., Crivellaro, A.,  
357 Reinig, F., Tegel, W., Kirilyanov, A., Trnka, M., & Oppenheimer, C. (2022). Global tree-  
358 ring response and inferred climate variation following the mid-thirteenth century Samalas  
359 eruption. *Climate Dynamics*, 59(1), 531–546. [https://doi.org/10.1007/s00382-022-06141-](https://doi.org/10.1007/s00382-022-06141-3)  
360 [3](https://doi.org/10.1007/s00382-022-06141-3)
- 361 Burgisser, A. (2005). Physical volcanology of the 2,050 bp caldera-forming eruption of Okmok  
362 volcano, Alaska. *Bulletin of Volcanology*, 67(6), 497–525.  
363 <https://doi.org/10.1007/s00445-004-0391-5>
- 364 Burke, A., Moore, K. A., Sigl, M., Nita, D. C., McConnell, J. R., & Adkins, J. F. (2019).  
365 Stratospheric eruptions from tropical and extra-tropical volcanoes constrained using high-  
366 resolution sulfur isotopes in ice cores. *Earth and Planetary Science Letters*, 521, 113–  
367 119. <https://doi.org/10.1016/j.epsl.2019.06.006>
- 368 Cadoux, A., Scaillet, B., Bekki, S., Oppenheimer, C., & Druitt, T. H. (2015). Stratospheric  
369 Ozone destruction by the Bronze-Age Minoan eruption (Santorini Volcano, Greece).  
370 *Scientific Reports*, 5(1), Article 1. <https://doi.org/10.1038/srep12243>
- 371 Costa, F., Scaillet, B., & Gougaud, A. (2003). Massive atmospheric sulfur loading of the AD  
372 1600 Huaynaputina eruption and implications for petrologic sulfur estimates.  
373 *Geophysical Research Letters*, 30(2). <https://doi.org/10.1029/2002GL016402>
- 374 DallaSanta, K., & Polvani, L. M. (2022). Volcanic stratospheric injections up to 160 Tg(S) yield  
375 a Eurasian winter warming indistinguishable from internal variability. *Atmospheric*  
376 *Chemistry and Physics*, 22(13), 8843–8862. <https://doi.org/10.5194/acp-22-8843-2022>

- 377 Devine, J. D., Sigurdsson, H., Davis, A. N., & Self, S. (1984). Estimates of sulfur and chlorine  
378 yield to the atmosphere from volcanic eruptions and potential climatic effects. *Journal of*  
379 *Geophysical Research: Solid Earth*, 89(B7), 6309–6325.  
380 <https://doi.org/10.1029/JB089iB07p06309>
- 381 Dietterich, H., & de Silva, S. (2010). Sulfur yield of the 1600 eruption of Huaynaputina, Peru:  
382 Contributions from magmatic, fluid-phase, and hydrothermal sulfur. *Journal of*  
383 *Volcanology and Geothermal Research*, 197(1), 303–312.  
384 <https://doi.org/10.1016/j.jvolgeores.2010.01.003>
- 385 Dufek, J., Manga, M., & Staedter, M. (2007). Littoral blasts: Pumice-water heat transfer and the  
386 conditions for steam explosions when pyroclastic flows enter the ocean. *Journal of*  
387 *Geophysical Research: Solid Earth*, 112(B11). <https://doi.org/10.1029/2006JB004910>
- 388 Dull, R. A., Southon, J. R., Kutterolf, S., Anchukaitis, K. J., Freundt, A., Wahl, D. B., Sheets, P.,  
389 Amaroli, P., Hernandez, W., Wiemann, M. C., & Oppenheimer, C. (2019). Radiocarbon  
390 and geologic evidence reveal Ilopango volcano as source of the colossal ‘mystery’  
391 eruption of 539/40 CE. *Quaternary Science Reviews*, 222, 105855.  
392 <https://doi.org/10.1016/j.quascirev.2019.07.037>
- 393 Fell, H. G., Baldini, J. U. L., Dodds, B., & Sharples, G. J. (2020). Volcanism and global plague  
394 pandemics: Towards an interdisciplinary synthesis. *Journal of Historical Geography*, 70,  
395 36–46. <https://doi.org/10.1016/j.jhg.2020.10.001>
- 396 Finney, B., Turner, S., Hawkesworth, C., Larsen, J., Nye, C., George, R., Bindeman, I., &  
397 Eichelberger, J. (2008). Magmatic Differentiation at an Island-arc Caldera: Okmok  
398 Volcano, Aleutian Islands, Alaska. *Journal of Petrology*, 49(5), 857–884.  
399 <https://doi.org/10.1093/petrology/egn008>



- 400 Gerlach, T. M., Westrich, H. R., Symonds, R. B., Newhall, C. G., & Punongbayan, R. S. (1996).  
401 Pre-eruption vapor in magma of the climactic Mount Pinatubo eruption: Source of the  
402 giant stratospheric sulfur dioxide cloud. In *Fire and Mud. Eruptions and Lahars of Mount*  
403 *Pinatubo, Philippines* (pp. 415–434). University of Washington Press.
- 404 Gertisser, R., Self, S., Thomas, L. E., Handley, H. K., Van Calsteren, P., & Wolff, J. A. (2012).  
405 Processes and Timescales of Magma Genesis and Differentiation Leading to the Great  
406 Tambora Eruption in 1815. *Journal of Petrology*, *53*(2), 271–297.  
407 <https://doi.org/10.1093/petrology/egr062>
- 408 Guillet, S., Corona, C., Stoffel, M., Khodri, M., Lavigne, F., Ortega, P., Eckert, N., Sielenou, P.  
409 D., Daux, V., Churakova (Sidorova), O. V., Davi, N., Edouard, J.-L., Zhang, Y.,  
410 Luckman, B. H., Myglan, V. S., Guiot, J., Beniston, M., Masson-Delmotte, V., &  
411 Oppenheimer, C. (2017). Climate response to the Samalas volcanic eruption in 1257  
412 revealed by proxy records. *Nature Geoscience*, *10*(2), Article 2.  
413 <https://doi.org/10.1038/ngeo2875>
- 414 Guo, S., Bluth, G. J. S., Rose, W. I., Watson, I. M., & Prata, A. J. (2004). Re-evaluation of SO<sub>2</sub>  
415 release of the 15 June 1991 Pinatubo eruption using ultraviolet and infrared satellite  
416 sensors. *Geochemistry, Geophysics, Geosystems*, *5*(4).  
417 <https://doi.org/10.1029/2003GC000654>
- 418 Hauri, E., Wang, J., Dixon, J. E., King, P. L., Mandeville, C., & Newman, S. (2002). SIMS  
419 analysis of volatiles in silicate glasses: 1. Calibration, matrix effects and comparisons  
420 with FTIR. *Chemical Geology*, *183*(1), 99–114. [https://doi.org/10.1016/S0009-](https://doi.org/10.1016/S0009-2541(01)00375-8)  
421 [2541\(01\)00375-8](https://doi.org/10.1016/S0009-2541(01)00375-8)

- 422 Iacovino, K., Ju-Song, K., Sisson, T., Lowenstern, J., Kuk-Hun, R., Jong-Nam, J., Kun-Ho, S.,  
423 Song-Hwan, H., Oppenheimer, C., Hammond, J. O. S., Donovan, A., Liu, K. W., &  
424 Kum-Ran, R. (2016). Quantifying gas emissions from the “Millennium Eruption” of  
425 Paektu volcano, Democratic People’s Republic of Korea/China. *Science Advances*, 2(11),  
426 e1600913. <https://doi.org/10.1126/sciadv.1600913>
- 427 Larsen, J. F., Neal, C., Schaefer, J., Beget, J., & Nye, C. (2007). Late Pleistocene and Holocene  
428 Caldera-Forming Eruptions of Okmok Caldera, Aleutian Islands, Alaska. In *Volcanism*  
429 *and Subduction: The Kamchatka Region* (pp. 343–364). American Geophysical Union  
430 (AGU). <https://doi.org/10.1029/172GM24>
- 431 Lloyd, A. S., Plank, T., Ruprecht, P., Hauri, E. H., & Rose, W. (2013). Volatile loss from melt  
432 inclusions in pyroclasts of differing sizes. *Contributions to Mineralogy and Petrology*,  
433 165(1), 129–153. <https://doi.org/10.1007/s00410-012-0800-2>
- 434 Luterbacher, J., Werner, J. P., Smerdon, J. E., Fernández-Donado, L., González-Rouco, F. J.,  
435 Barriopedro, D., Ljungqvist, F. C., Büntgen, U., Zorita, E., Wagner, S., Esper, J.,  
436 McCarroll, D., Toreti, A., Frank, D., Jungclaus, J. H., Barriendos, M., Bertolin, C.,  
437 Bothe, O., Brázdil, R., ... Zerefos, C. (2016). European summer temperatures since  
438 Roman times. *Environmental Research Letters*, 11(2), 024001.  
439 <https://doi.org/10.1088/1748-9326/11/2/024001>
- 440 Mandeville, C. W., Carey, S., & Sigurdsson, H. (1996). Magma mixing, fractional crystallization  
441 and volatile degassing during the 1883 eruption of Krakatau volcano, Indonesia. *Journal*  
442 *of Volcanology and Geothermal Research*, 74(3), 243–274.  
443 [https://doi.org/10.1016/S0377-0273\(96\)00060-1](https://doi.org/10.1016/S0377-0273(96)00060-1)

- 444 Marshall, L. R., Schmidt, A., Johnson, J. S., Mann, G. W., Lee, L. A., Rigby, R., & Carslaw, K.  
445 S. (2021). Unknown Eruption Source Parameters Cause Large Uncertainty in Historical  
446 Volcanic Radiative Forcing Reconstructions. *Journal of Geophysical Research:*  
447 *Atmospheres*, 126(13), e2020JD033578. <https://doi.org/10.1029/2020JD033578>
- 448 McConnell, J. R., Sigl, M., Plunkett, G., Burke, A., Kim, W. M., Raible, C. C., Wilson, A. I.,  
449 Manning, J. G., Ludlow, F., Chellman, N. J., Innes, H. M., Yang, Z., Larsen, J. F.,  
450 Schaefer, J. R., Kipfstuhl, S., Mojtabavi, S., Wilhelms, F., Opel, T., Meyer, H., &  
451 Steffensen, J. P. (2020). Extreme climate after massive eruption of Alaska's Okmok  
452 volcano in 43 BCE and effects on the late Roman Republic and Ptolemaic Kingdom.  
453 *Proceedings of the National Academy of Sciences*, 117(27), 15443–15449.  
454 <https://doi.org/10.1073/pnas.2002722117>
- 455 Orbe, C., Rind, D., Jonas, J., Nazarenko, L., Faluvegi, G., Murray, L. T., Shindell, D. T.,  
456 Tsigaridis, K., Zhou, T., Kelley, M., & Schmidt, G. A. (2020). GISS Model E2.2: A  
457 Climate Model Optimized for the Middle Atmosphere—2. Validation of Large-Scale  
458 Transport and Evaluation of Climate Response. *Journal of Geophysical Research:*  
459 *Atmospheres*, 125(24), e2020JD033151. <https://doi.org/10.1029/2020JD033151>
- 460 Pauling, A. G., Bitz, C. M., & Armour, K. C. (2023). The Climate Response to the Mt. Pinatubo  
461 Eruption Does Not Constrain Climate Sensitivity. *Geophysical Research Letters*, 50(7),  
462 e2023GL102946. <https://doi.org/10.1029/2023GL102946>
- 463 Peccia, A., Moussallam, Y., & Plank, T. (2023). Melt inclusion and matrix glass data from the 43  
464 BCE eruption of Okmok Volcano (Version 1.0). Interdisciplinary Earth Data Alliance  
465 (IEDA). <https://doi.org/10.26022/IEDA/112955>

- 466 Pouget, M., Moussallam, Y., Rose-Koga, E., Sigurdsson, H., Carey, S., & Kelley, K. (in prep). A  
467 reassessment of the sulfur, chlorine and fluorine atmospheric loading during the 1815  
468 Tambora eruption. *Bulletin of Volcanology*.
- 469 Rind, D., Orbe, C., Jonas, J., Nazarenko, L., Zhou, T., Kelley, M., Lacis, A., Shindell, D.,  
470 Faluvegi, G., Romanou, A., Russell, G., Tausnev, N., Bauer, M., & Schmidt, G. (2020).  
471 GISS Model E2.2: A Climate Model Optimized for the Middle Atmosphere—Model  
472 Structure, Climatology, Variability, and Climate Sensitivity. *Journal of Geophysical  
473 Research: Atmospheres*, 125(10), e2019JD032204.  
474 <https://doi.org/10.1029/2019JD032204>
- 475 Robock, A. (2000). Volcanic eruptions and climate. *Reviews of Geophysics*, 38(2), 191–219.  
476 <https://doi.org/10.1029/1998RG000054>
- 477 Rowell, C. R., Jellinek, A. M., Hajimirza, S., & Aubry, T. J. (2022). External Surface Water  
478 Influence on Explosive Eruption Dynamics, With Implications for Stratospheric Sulfur  
479 Delivery and Volcano-Climate Feedback. *Frontiers in Earth Science*, 10. Retrieved from  
480 <https://www.frontiersin.org/articles/10.3389/feart.2022.788294>
- 481 Scaillet, B., Clemente, B., Evans, B. W., & Pichavant, M. (1998). Redox control of sulfur  
482 degassing in silicic magmas. *Journal of Geophysical Research: Solid Earth*, 103(B10),  
483 23937–23949. <https://doi.org/10.1029/98JB02301>
- 484 Schmidt, A., Ostro, B., Carslaw, K. S., Wilson, M., Thordarson, T., Mann, G. W., & Simmons,  
485 A. J. (2011). Excess mortality in Europe following a future Laki-style Icelandic eruption.  
486 *Proceedings of the National Academy of Sciences*, 108(38), 15710–15715.  
487 <https://doi.org/10.1073/pnas.1108569108>

- 488 Self, S., & King, A. J. (1996). Petrology and sulfur and chlorine emissions of the 1963 eruption  
489 of Gunung Agung, Bali, Indonesia. *Bulletin of Volcanology*, 58(4), 263–285.  
490 <https://doi.org/10.1007/s004450050139>
- 491 Sigl, M., Winstrup, M., McConnell, J. R., Welten, K. C., Plunkett, G., Ludlow, F., Büntgen, U.,  
492 Caffee, M., Chellman, N., Dahl-Jensen, D., Fischer, H., Kipfstuhl, S., Kostick, C.,  
493 Maselli, O. J., Mekhaldi, F., Mulvaney, R., Muscheler, R., Pasteris, D. R., Pilcher, J. R.,  
494 ... Woodruff, T. E. (2015). Timing and climate forcing of volcanic eruptions for the past  
495 2,500 years. *Nature*, 523(7562), Article 7562. <https://doi.org/10.1038/nature14565>
- 496 Smith, V. C., Costa, A., Aguirre-Díaz, G., Pedrazzi, D., Scifo, A., Plunkett, G., Poret, M.,  
497 Tournigand, P.-Y., Miles, D., Dee, M. W., McConnell, J. R., Sunyé-Puchol, I., Harris, P.  
498 D., Sigl, M., Pilcher, J. R., Chellman, N., & Gutiérrez, E. (2020). The magnitude and  
499 impact of the 431 CE Tierra Blanca Joven eruption of Ilopango, El Salvador.  
500 *Proceedings of the National Academy of Sciences*, 117(42), 26061–26068.  
501 <https://doi.org/10.1073/pnas.2003008117>
- 502 Su, Y., Huber, C., Bachmann, O., Zajacz, Z., Wright, H., & Vazquez, J. (2016). The role of  
503 crystallization-driven exsolution on the sulfur mass balance in volcanic arc magmas.  
504 *Journal of Geophysical Research: Solid Earth*, 121(8), 5624–5640.  
505 <https://doi.org/10.1002/2016JB013184>
- 506 Tan, M., Liu, T., Hou, J., Qin, X., Zhang, H., & Li, T. (2003). Cyclic rapid warming on  
507 centennial-scale revealed by a 2650-year stalagmite record of warm season temperature.  
508 *Geophysical Research Letters*, 30(12). <https://doi.org/10.1029/2003GL017352>
- 509 Thordarson, T., Miller, D. J., Larsen, G., Self, S., & Sigurdsson, H. (2001). New estimates of  
510 sulfur degassing and atmospheric mass-loading by the 934 AD Eldgjá eruption, Iceland.

- 511 *Journal of Volcanology and Geothermal Research*, 108(1), 33–54.  
512 [https://doi.org/10.1016/S0377-0273\(00\)00277-8](https://doi.org/10.1016/S0377-0273(00)00277-8)
- 513 Thordarson, T., & Self, S. (2003). Atmospheric and environmental effects of the 1783–1784  
514 Laki eruption: A review and reassessment. *Journal of Geophysical Research:*  
515 *Atmospheres*, 108(D1), AAC 7-1-AAC 7-29. <https://doi.org/10.1029/2001JD002042>
- 516 Thordarson, T., Self, S., Óskarsson, N., & Hulsebosch, T. (1996). Sulfur, chlorine, and fluorine  
517 degassing and atmospheric loading by the 1783–1784 AD Laki (Skaftár Fires) eruption in  
518 Iceland. *Bulletin of Volcanology*, 58(2), 205–225. <https://doi.org/10.1007/s004450050136>
- 519 Toohey, M., & Sigl, M. (2017). Volcanic stratospheric sulfur injections and aerosol optical depth  
520 from 500 BCE to 1900 CE. *Earth System Science Data*, 9(2), 809–831.  
521 <https://doi.org/10.5194/essd-9-809-2017>
- 522 Toohey, M., Stevens, B., Schmidt, H., & Timmreck, C. (2016). Easy Volcanic Aerosol (EVA  
523 v1.0): An idealized forcing generator for climate simulations. *Geoscientific Model*  
524 *Development*, 9(11), 4049–4070. <https://doi.org/10.5194/gmd-9-4049-2016>
- 525 Toplis, M. J. (2005). The thermodynamics of iron and magnesium partitioning between olivine  
526 and liquid: criteria for assessing and predicting equilibrium in natural and experimental  
527 systems. *Contributions to Mineralogy and Petrology*, 149(1), 22–39.  
528 <https://doi.org/10.1007/s00410-004-0629-4>
- 529 Vidal, C. M., Métrich, N., Komorowski, J.-C., Pratomo, I., Michel, A., Kartadinata, N., Robert,  
530 V., & Lavigne, F. (2016). The 1257 Samalas eruption (Lombok, Indonesia): The single  
531 greatest stratospheric gas release of the Common Era. *Scientific Reports*, 6(1), 34868.  
532 <https://doi.org/10.1038/srep34868>

- 533 Waters, L. E., & Lange, R. A. (2015). An updated calibration of the plagioclase-liquid  
534 hygrometer-thermometer applicable to basalts through rhyolites. *American Mineralogist*,  
535 100(10), 2172–2184. <https://doi.org/10.2138/am-2015-5232>
- 536 Witter, J. B., & Self, S. (2007). The Kuwae (Vanuatu) eruption of AD 1452: Potential magnitude  
537 and volatile release. *Bulletin of Volcanology*, 69(3), 301–318.  
538 <https://doi.org/10.1007/s00445-006-0075-4>
- 539 Wolfe, B. A. (2001). *Paleohydrology of a catastrophic flood release from Okmok caldera and*  
540 *post-flood eruption history at Okmok Volcano, Umnak Island, Alaska* [Thesis].  
541 <https://scholarworks.alaska.edu/handle/11122/6716>
- 542 Zambri, B., Robock, A., Mills, M. J., & Schmidt, A. (2019). Modeling the 1783–1784 Laki  
543 Eruption in Iceland: 2. Climate Impacts. *Journal of Geophysical Research: Atmospheres*,  
544 124(13), 6770–6790. <https://doi.org/10.1029/2018JD029554>
- 545 Zimmer, M. M., Plank, T., Hauri, E. H., Yogodzinski, G. M., Stelling, P., Larsen, J., Singer, B.,  
546 Jicha, B., Mandeville, C., & Nye, C. J. (2010). The Role of Water in Generating the Calc-  
547 alkaline Trend: New Volatile Data for Aleutian Magmas and a New Tholeiitic Index.  
548 *Journal of Petrology*, 51(12), 2411–2444. <https://doi.org/10.1093/petrology/egq062>